White Rose Research Online

eprints@whiterose.ac.uk
https://eprints.whiterose.ac.uk
Universities of Leeds, Sheffield and York

Deposited via The University of Sheffield.

White Rose Research Online URL for this paper:
https://eprints.whiterose.ac.uk/id/eprint/247321/

Version: Published Version

Article:
Passmore, C., Parnell, A.J., Howse, J.R. et al. (2026) High throughput manufacture of colloidal crystal monolayers with optimisable crystallinity. Scientific Reports. ISSN: 2045-2322

https://doi.org/10.1038/s41598-026-71838-y

Reuse
This article is distributed under the terms of the Creative Commons Attribution (CC BY) licence. This licence allows you to distribute, remix, tweak, and build upon the work, even commercially, as long as you credit the authors for the original work. More information and the full terms of the licence here: https://creativecommons.org/licenses/

Takedown
If you consider content in White Rose Research Online to be in breach of UK law, please notify us by emailing eprints@whiterose.ac.uk including the URL of the record and the reason for the withdrawal request.

UNIVERSITY OF LEEDS
University of Sheffield
UNIVERSITY of York

ARTICLE | Article in Press

High throughput manufacture of colloidal crystal monolayers with optimisable crystallinity

Christopher Passmore · Andrew J. Parnell · Jonathan R. Howse · Stephen J. Ebbens

Received: 4 May 2026 / Accepted: 11 September 2026
© The Author(s) 2026

Abstract

The unique optical and structural properties of colloidal crystal monolayers offer great potential for integration into batteries, solar panels, and sensors. However, commercial adoption is limited by manufacturing challenges. Conventional methods such as Langmuir-Blodgett deposition, spin coating, and drop casting are batch processes and are intrinsically slow. In this context we demonstrate that roll-to-roll slot die coating is a scalable, reproducible, and high throughput alternative for continuous manufacture of colloidal crystals. By using multi-scale characterisation tools to quantify long range order, we show that roll-to-roll slot die coating can produce hexagonal close packed crystalline colloid domains with long range order that can be varied via control of the substrate velocity. This tuneability offers a route to adjust material properties for specific functional applications that is compatible with self-optimising and closed loop control approaches. Slot die coating consequently has the potential to radically improve 2D colloidal crystal fabrication speed and repeatability and consequently unlock new opportunities for advanced device manufacture.

Introduction

Periodically ordered 2D and 3D arrays of colloidal particles, known as colloidal crystals, have emerged as key materials for a range of advanced technologies[1], including photonic devices[2], anti-reflective coatings[3], sensors[4], battery separators[5], and energy-harvesting systems[6]. Colloidal crystals' unique properties arise from the precise regular arrangement of particles. Crystalline particle arrangements are typically formed by the self-assembly of colloidal suspensions that satisfy specific criteria including low polydispersity, appropriate volume fraction, and well-tuned inter-particle forces[7,8]. While self-assembly can occur across a wide range of length scales, sub-micron sized particles are of particular interest as colloidal monolayers in this size regime have potential to improve performance in many key technologies such as dye-sensitized solar cells[9]and anode structures for lithium ion batteries[10,11].

Despite their promise as next generation materials, colloidal crystals are yet to be integrated into readily available commercial devices. The mass manufacture of high quality colloidal crystals has often been highlighted as a critical limiting factor for real world applications[12–14]. Conventional laboratory-scale techniques such as spin coating[15], drop casting[11,16], and Langmuir-Blodgett deposition[17] offer limited control over film uniformity and

This Article in Press is shared early to give you faster access to new research. It is citable and carries a permanent DOI. The final edited version will replace it automatically.



https://doi.org/10.1038/s41598-026-71838-y

Published online: 21 September 2026

scientific reports

crystallinity, and suffer from slow deposition speeds (~50 μm/s), rendering them unsuitable for high-throughput production[18–20].

Recent efforts to scale up colloidal crystal fabrication using roll-to-roll wire bar coating have shown promise, but still face challenges[21,22]. For example, Cagnani *et al.* used a roll-to-roll wire bar method to manufacture large area colloidal crystals monolayers, yet reported significant colloid loss (~26 %) during this process, and limited means to alter the colloidal crystal quality by varying processing parameters[21]. Specifically, the crystal domain size and number of dislocation defects were not found to be controlled by the fluid pump rate[21]. Because the desirable properties of colloidal crystals depend sensitively on their degree of order, and the type and amount defects[23,24], there remains a critical need for a manufacturing method that allows fine control over crystal structure while conserving material and enabling industrial scale production.

Roll-to-roll slot die coating presents an alternative thin film manufacturing method[25]. Slot die coating is a high throughput (up to 2 m/s substrate velocity[26]), solution-based deposition method which deposits a uniform coating onto a moving substrate by pumping fluid through a precisely machined slot in the printing head[27]. Slot die coating offers a potentially versatile method of manufacturing colloidal crystals, and is compatible with a wide range of solvents, colloids and self-assembly mechanisms. Additionally, slot die coating offers an ability to precisely tune the wet coating thickness by varying the fluid pump rate and substrate velocity, as it is a fully metered process[27–29]. As the colloidal crystal structure is extremely sensitive to the areal coverage of colloids, accurate metering of the deposited solution is an attractive feature, as it allows the deposited particle density to be reliably defined and varied for a known volume fraction ink[30,31]. Therefore, slot die coating can potentially offer versatile manufacture of colloidal coatings with different structures using the same production equipment and solution formulation. Furthermore, compared with other thin film manufacturing techniques, such as doctor blade coating, slot die coating has been found to offer better control over coating width and thickness and uniformity[27].

This article presents the first, to our knowledge, successful fabrication of large area colloidal crystal monolayers using continuous roll-to-roll slot die coating. While a wide range of parameters such as coating gap, substrate temperature, colloidal size, composition and polydispersity alter coating quality, in this study we focus on independently adjusting substrate velocity and pump rate, based on the expectation that areal coverage will be the key colloid monolayer quality determining factor. The ability to exert control over the colloidal crystal structure demonstrated here by changing the ratio of pump rate to substrate velocity, considerably expands on the previous doctor blade study in this respect. The manufactured coatings are evaluated using multi-scale characterisation by optical microscopy and SEM, revealing both the overall coating quality and the colloidal packing arrangements with single particle resolution. Quantitative 2D bond-orientational autocorrelation analysis demonstrates that the long range hexagonal ordering is tuneable via altering the substrate velocity, with a constant pump rate and coating solution formulation. These findings provide a pathway toward roll-to-roll production of colloidal crystals with tunable structural properties, advancing the route towards scalable device manufacturing.

Results

The 300 nm SiO_2 colloidal solutions were prepared as per the Methods Section. After that, the solution was applied to a transparent PET substrate using a roll-to-roll slot die coater combined with continuous agitation. The vibrating motor and magnetic stirrer were effective in minimising the aggregation, sedimentation and jamming[32]of colloids. Without these components the final coatings contained streaks and large defects[33]. Having achieved high quality coatings, we systematically investigated the effect of coating parameters as described below.

Systematic parameter changes of roll-to-roll slot die coating colloidal solution

An important advantage of slot die coating over other thin film manufacturing techniques is the ability to precisely adjust the wet coating thickness[27]. In the context of coating colloidal dispersions, an increase in wet coat thickness, for a given formulation, necessarily leads to a higher colloidal areal density in the final dried coating. In Fig. 1, the effect of increasing the colloidal coverage by this mechanism on dried coating structure is shown; reducing the substrate velocity from 11 mm/s to 7 mm/s, while the pump rate is kept constant at 4.5 mL/hr. The coating gap, which can also alter coating features, was kept constant at an optimised value of 0.5 mm. The quantitative effect of varying substrate velocity on wet coating thickness is described by $t = Q/Vw$, where t is wet coating thickness, Q in volumetric flow rate, V is substrate velocity and $w$is coating width[34]. Hence it can be seen that as substrate velocity decreases at fixed volumetric flow rate, the coating thickness is expected to increase, assuming coating width remains constant. For our coatings, this increase in wet coating thickness will also lead to an increased coverage of colloids in the dried film.

Considering the overall coating quality depicted in the wide angle images at the top of Fig. 1, the central region of the coating appears uniform, and free from streaks and defects associated with aggregation. These images reflect the coating's appearance between 45 to 70 s after deposition on the substrate (drying time is dependant on substrate velocity: the camera is focused on a point 500 mm from the slot die head), so reflect a partially dry state. Line profiles through typical cross-sections of these wide-angle images are shown in Fig. 2. Variations in reflected light intensity confirm the relative homogeneity of the central area of the coating, and also accentuate the coating's edge effects. The coating's boundaries with the substrate are seen as pronounced double peaked increases in intensity. This contrast likely reflects increased accumulations of colloids at the edge of the coating, often termed the coffee ring effect[35]. For many thin film applications, it is common practice to cut off the edges of coatings prior to use, to avoid this artefact, leading to waste during processing. It is also apparent both from Fig. 1 and Fig. 2 that as the substrate velocity decreases relative to pump rate, the coating width progressively increases. This is in contrast to the coating theory outlined above which commonly assumes the coating width is independent of the amount of fluid supplied when the coating is within the operating window. In reality, higher pump rates relative to substrate speed also produce increased wetting of the substrate. This wetting feature is consistently revealed by our imaging system for various different coatings and parameters.

Although slot-die coating is conventionally treated as a well-metered process with coating width fixed by the die geometry, the lateral position of the coating meniscus can be influenced by capillary flow and is not necessarily fixed without additional meniscus control; consequently, increasing flow rate may promote transverse spreading

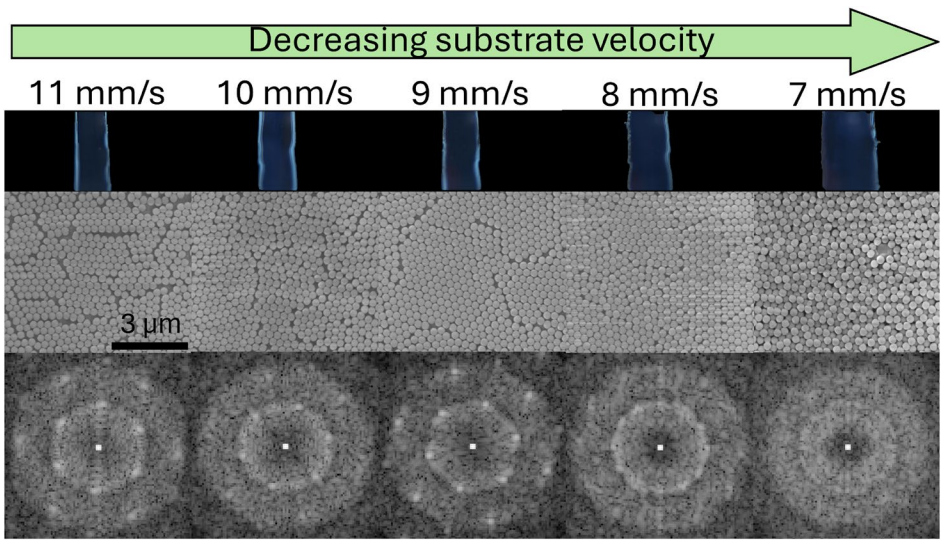


Fig. 1 Effect of substrate velocity on colloidal crystals obtained over a range of length scales. The top row shows images of the entire coating width, with a field of view of 50 mm. The second row shows SEM images from the center of the coated area and the third row displays corresponding fast Fourier transforms of the SEM images showing the degree of order.

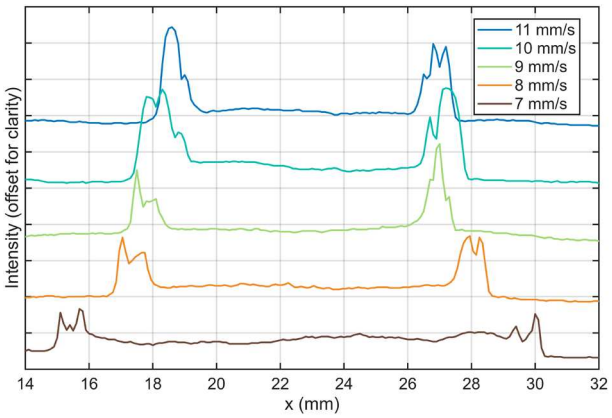


Fig. 2 Line profiles of intensities extracted from wide angle images in Fig. 1.

and an increase in wetted width. In addition, the rheological behaviour of the colloidal suspension and shear experienced during coating may influence flow and subsequent drying-driven redistribution, particularly as local particle concentration increases during evaporation. These effects were not independently characterised here, but may also contribute to the observed changes in coating width and edge profile. The progressively reduced relative prominence of the edge features at lower substrate velocities in Fig. 2 may therefore reflect changes in the balance between transverse spreading, drying-driven redistribution and suspension rheology, although the present measurements do not allow these individual contributions to be separated.

Inspection of the higher resolution SEM images in Fig. 1reveal the corresponding differences in the colloidal packing at single particle resolution (SEM images were chosen to be representative of the centre of the coated area)[34]. For example, as the substrate velocity decreases from 11 mm/s to 9 mm/s, the hexagonal close packed colloidal crystal domain size increases and the amount of dislocations at the boundaries between domains decreases. The 9 mm/s coating shows the largest domain sizes and lowest amount of defects. This behaviour reflects the balance between the hydrodynamic transport of the colloids during coating and the interparticle interactions that drive self-assembly, with attractive/repulsive surface forces and electrostatic interactions influencing the extent to which particles can rearrange into a close-packed configuration as the film dries. At the intermediate coating conditions, the reduced areal loading and sufficient particle mobility appear to provide a favourable balance between particle rearrangement and deposition, promoting larger ordered domains, whereas excessive loading at lower substrate velocities restricts rearrangement and promotes buckling and secondary-layer formation. From 9 mm/s to 7 mm/s, the colloidal crystal goes from being a monolayer to a layer with a slight buckle, with some colloids sitting slightly higher than the others, to a partial secondary layer at a velocity of 7 mm/s. This is as expected as these conditions correspond to overloading the colloids relative to the available substrate area. It is worth noting that while these trends in monolayer structure are consistent with a simple conservation of mass argument, the real world system has additional complexity. As already remarked upon, changes in coating width associated with changes in substrate velocity also occur, and the film profiles when partially dry also differ from a simple box profile, (see Fig. 2) so in reality it is the interplay of these factors that are leading to the changes in areal density and associated crystal packing.

In Fig. 3 the top row depicts the Voronoi colour coding of the hexagonal order over large regions of the coating. The colour coding corresponds to the local hexagonal lattice orientation obtained from Voronoi tessellation, where each domain is assigned a colour based on the angular orientation of nearest-neighbour bonds. It is apparent that in the 10 mm/s to 8 mm/s range distinct aligned ordered domains are observed, these are less well defined at 11 mm/s and not present at 7 mm/s. The low magnification SEM images that were used to generate this coding are displayed in Supplementary Fig. S6.

Figure 3 also shows bond-orientational autocorrelation analysis to assess the long range order in the samples. This analysis only assesses the amount of hexagonal close packed order, so alternative packing types are not accounted for. For a perfectly ordered structure, $g_6(r)$ remains close to 1 over all distances, whereas a rapidly

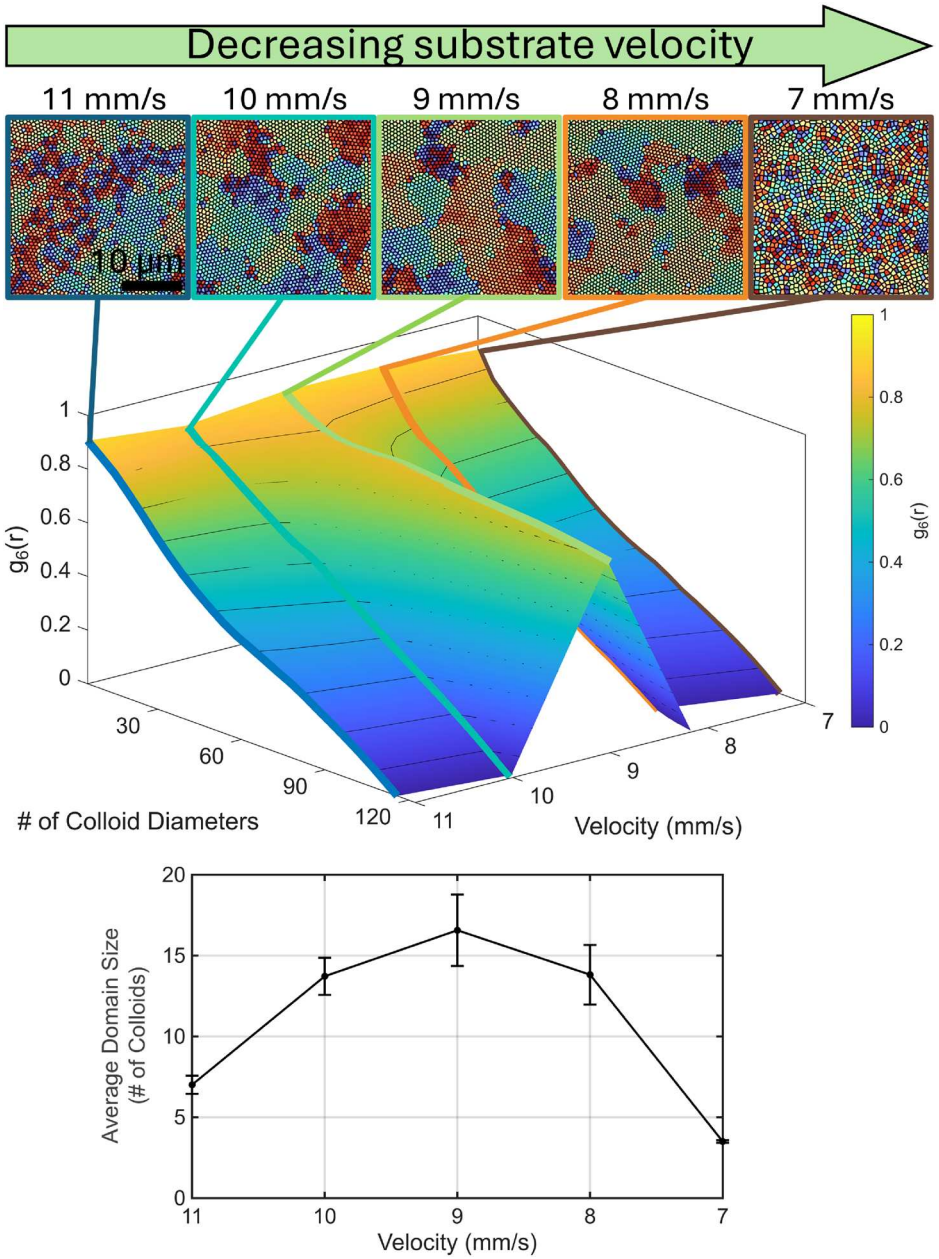


Fig. 3 Lower magnification SEM images were of the samples in Fig 1. Partial Voronoi plots of these SEM images are shown, with different colours within the Voronoi plots showing different colloidal crystal orientation. Autocorrelation analysis of the low magnification SEM images was conducted. $g_6(r)$ is the 2D autocorrelation function, a measure of the degree of crystallinity in the colloidal crystal. The average grain size was extracted and is displayed in the lower graph, with standard error shown by the error bars. The full SEM images and Voronoi plots are shown in Supplementary Fig. S6.

decaying function indicates a lack of long-range order. r is distance in colloid diameter. This analysis extends to 125 colloidal diameters and hence insights into the long range order are revealed. Figure 3 supports the qualitative conclusion made by direct inspection of the high magnification SEM images, that coating at 9 mm/s gives the highest quality colloidal crystal monolayer, and this figure also suggests this bond-orientation coating property has a distinct optimum that can be accessed by varying the substrate velocity, in a way that could be used to enable automated self-optimising manufacture.

Having determined that varying colloidal areal density via changes in substrate velocity at fixed pump rate can control colloidal order, we now consider the alternative strategy, to change pump rate at a fixed substrate velocity. We arranged the experimental parameters to access an overlapping range of pump rate to substrate velocity ratios, but at a higher fixed substrate velocity of 12 mm/s. This additional experiment consequently tests if the absolute magnitude of parameters alters behaviour, in addition to their relative values. The effect of pump rate, on the colloidal crystal obtained is shown in Fig. 4. At 3.5 mL/hr a high density monolayer with hexagonal crystal

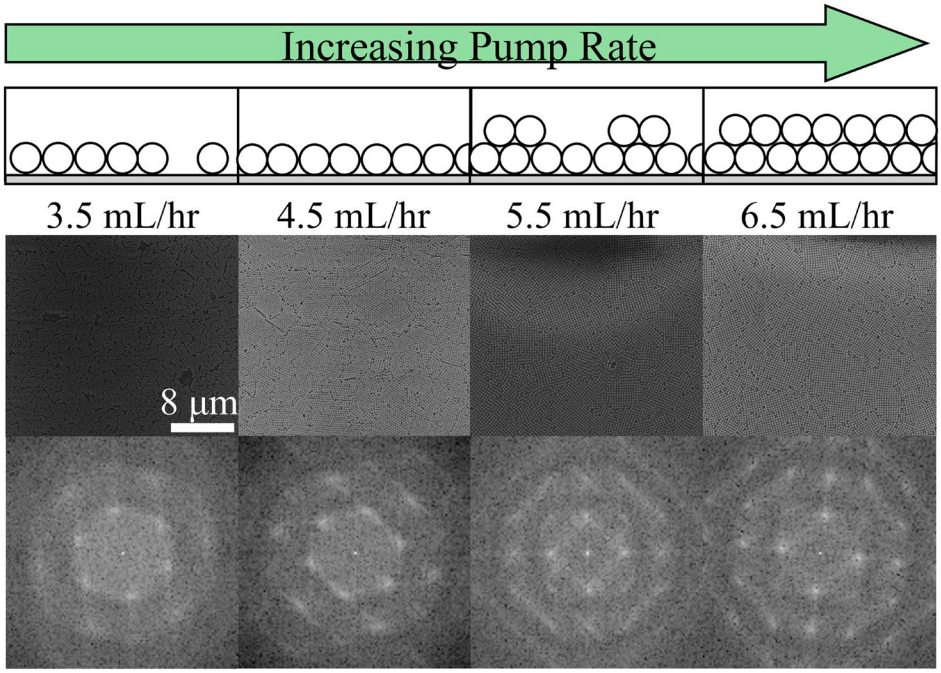


Fig. 4 Effect of pump rate on colloidal crystal ordering obtained for 300 nm SiO_2 colloids. The top row shows a schematic of the resultant coating as a function of pump rate. The second row shows SEM images from the center of the coated area and the third row displays corresponding fast Fourier transforms. Displayed images were chosen for how accurately they represented the majority of the sampled area.

packing is formed, with a high amount of dislocations and defects. At 4.5 mL/hr, the amount of uncovered patches is reduced, and the crystal is of higher quality. At 5.5 mL/hr, a partial secondary layer is formed and the packing type changes from hexagonal to square. At 6.5 mL/hr this partial secondary layer becomes more complete. At 6.5 mL/hr the packing type appears to be body centered cubic (bcc), with lower density than hexagonal packing (68 % compared to 74 %)[36]. The change in packing is further evidenced by the corresponding representative FFT images. These results suggest that under these coating conditions, beyond a critical areal coverage, the assembly mechanism transitions from 2D monolayer crystallisation to multilayer colloidal crystallisation, where alternative symmetries such as square and bcc-like ordering become accessible.

While the trend in crystal development initially matches the changing substrate velocity experiment: increasing areal coverage leads to more complete hexagonal packing; a divergence in behaviour is seen with a transition to a bcc like packing arrangement at the higher pump rate conditions. In addition, the congruence between conditions that have similar pump rate to substrate velocity ratios in both experiments can also be examined. For example the 5.5 mL/hr pump rate condition in Fig. 4 is equivalent to the substrate velocity 10 mm/s condition shown in Fig. 1 and 3, and likewise the 6.5 ml/hr pump rate condition in Fig. 4 can be compared with the 8 mm/s substrate velocity condition shown in Fig. 1 and 3. The differences between these coating structures shows that establishing a straightforward link between colloidal packing and pump rate:substrate velocity ratio is not possible, and suggests strongly that multivariate explorations, e.g. via a full Design of Experiments approach are required in the future to understand the structure-parameter relationships in more detail, as well as confirming the high sensitivity of self-assembly phenomena.

Taken together, these findings offer a clear demonstration of the ability to alter and optimise the colloidal monolayer structure by making small changes to specific in line coating parameters within established stable coating limits, however these results also illustrate the interplay between the many coating parameters is complex, and behaviour is not universally governed by a simple parametric ratio.

Even under optimised conditions, defects and disorder are present and can take many forms in 2D colloidal crystals[37]. Figure 5 summarises the types of defects observed in the final dried colloidal monolayers.

One type of defect observed are small pin holes in the monolayer. Debris on the substrate or non-uniform surface treatment may be the root cause, or alternatively these defects could be intrinsic to the self assembly mechanism. Another type of defect observed is a partial secondary layer. Potential causes for this type of defect include

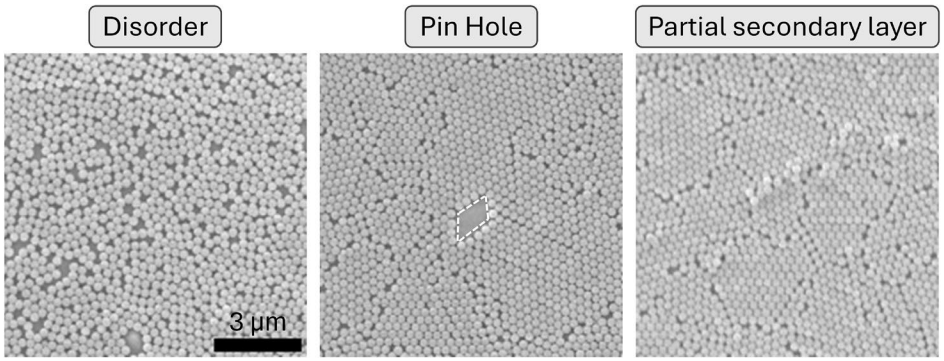


Fig. 5 SEM images showing the types of defects observed in the samples prepared using the roll-to-roll slot die coating with continuous agitation method. White dashed lines indicate the outline of the pin hole defect.

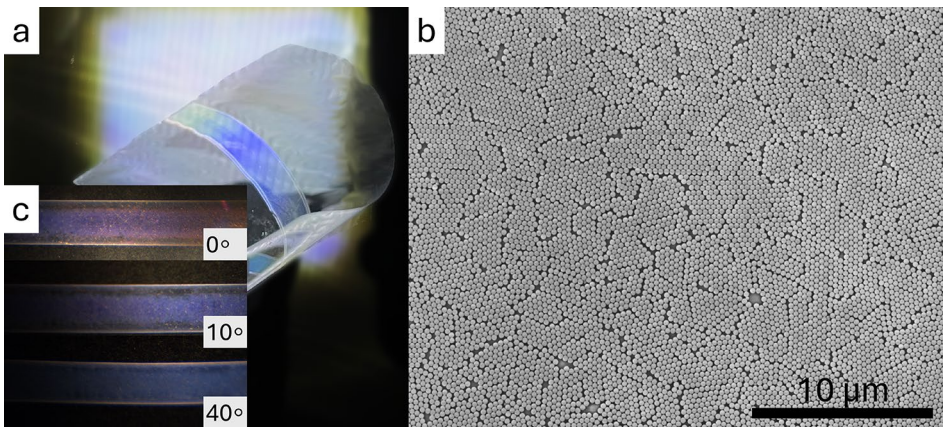


Fig. 6 **a** Image of colloidal monolayer obtained using 300 nm SiO_2 colloids. **b** SEM image of the sample. **c** Image of colloidal crystal coatings as a function of viewing angle, highlighting the iridescent colours. The experimental setups for image **a** and **c** are shown in Supplementary Figs. S4 and S5.

drying-driven flow (which also results in the "offee-ring"edge effects), coating bead instability and non-uniform dispersion of colloids within the coating solution. Disordered regions were also observed in certain areas of the sample between neighbouring colloidal crystal domains. As the size of individual domains increases, the relative impact of these diminishes, similar to observations during spin coating of colloidal crystals[15].

Defects are present in all real colloidal crystals, and our method appears to produce comparable quality colloidal crystals to other laboratory based methods, from starting materials of equivalent quality. It is anticipated that these defects can be reduced with better control over the environment, colloids, and substrate cleanliness, as is possible in larger scale optimised manufacturing facilities.

Macroscopic optical properties

The coating prepared in Fig. 6 used a pump rate of 4.5 mL/hr and substrate velocity of 9 mm/s, giving a 1:2 ratio of pump rate to substrate velocity and a theoretical wet coating thickness of 14 μm. This was selected for further attention, as it represents the highest quality colloidal crystal, as determined from the autocorrelation plot and inspection of SEM images. The SEM image in Fig. 6 **b** shows a large field of view with single particle resolution for this coating, confirming the slot die coated silica spheres exhibit a compact hexagonal arrangement over large regions. Visual inspection also revealed that under optimised illumination conditions the sample demonstrates colours, an observation that is typically associated with highly ordered 2D monolayers.

To investigate this further, 6 **a** shows a representative coating of approximately 300 nm SiO_2 colloids illuminated with collimated light. In the main left image, a range of colours are visible from red to yellow to green to blue as a function of the curvature of the large area 2D colloidal crystal, and hence viewing angle. This behaviour can be explained through optical diffraction from the ordered 2D colloidal array as described in Equation 1;

$$m\lambda = d_g n(\sin\theta_i + \sin\theta_m) \quad (1)$$

where d_g is the lattice spacing associated with the relevant diffraction direction, n is the refractive index of the surrounding medium which is 1 for 2D colloidal crystals in air, and θ_i and θ_m are the angles of incidence and diffraction, respectively. For a hexagonally ordered array, the relevant lattice spacing depends on the crystallographic direction considered. Grating diffraction relies on the 2D ordered array of particles for constructive interference to form structural colours.

Figure 6 **c** shows the colour change of the sample with viewing angle. For these images, the angle of both the incident light and viewing angle are changed symmetrically about the surface normal, as shown in Supplementary Fig. S4. Thin film interference and Bragg diffraction from the colloidal crystal can be used to describe this optical effect and is governed by Equation 2;

$$m\lambda = 2d_{111}n_{\text{eff}}\cos\theta_b \quad (2)$$

where d_{111} is the effective interplanar spacing, n_{eff} is the effective refractive index of the colloidal crystal, θ_b is the angle of propagation within the colloidal crystal and m is the diffraction order. Using the experimentally determined hydrodynamic particle diameter of approximately 320 nm and an effective refractive index of approximately 1.33, Equation 2 gives a characteristic reflection wavelength of approximately 700 nm at normal incidence, consistent with the observed red/pink colouration. The corresponding wavelength decreases with increasing angle, consistent with the observed progressive blue shift. The effective structural spacing is expected to be somewhat larger than the particle diameter because the colloids are not in direct contact within the deposited monolayer. The asymmetric silica/air/PET environment and the detailed two-dimensional packing are also expected to influence the precise optical response.

Materials and methods

Preparation of colloidal coating solutions

300 nm SiO_2 colloids were purchased from Pinfire (Germany) in a 36 wt% aqueous solution. 3.8 mL of this solution was dispersed in 30 g of absolute ethanol (99.8 % 32221 Sigma Aldrich, USA). The mixture underwent ultra-sonication in an ultrasonic bath (GT Sonic, China) and was then centrifuged using a 4K15 centrifuge (Sigma Laboratory, Germany) at 5000 rpm for 10 minutes for a series of five repeats, being re-dispersed in ethanol each time. This was done to remove the free water from the as received solution, with no thermal treatment applied.

A 10 wt% Tween 20 solution was prepared by adding Tween 20 (Sigma Aldrich, USA) to ethanol. 320 μL of this solution was added to the coating solution prepared above and the mixture underwent further agitation using a labDancer (IKA, Germany) and subsequent ultrasonication. This gave a concentration of 0.0006 g/mL of Tween 20 in the final coating solution.

The final coating solution had a concentration of 0.057 g/cm^3, which corresponds to a volume fraction of 0.021. The polydispersity index of the coating solution measured using a NANO-flex dynamic light scattering system (Colloid Metrix, Germany) was 9.1 % as shown in Supplementary Fig. S3. This is below 10 %, which is widely reported as the value above which colloidal assembly is significantly disrupted[30,38,39].

Immediately before coating, all colloidal solutions underwent approximately 30 seconds of vigorous shaking and ultra-sonication until sediment was no longer visible at the bottom of the container.

Roll-to-roll slot die coater

The roll-to-roll slot die coater was based on an in-house developed experimental rig which has been described previously[40,41], and is shown in Fig. 7. In summary, 36 μm thick polyethylene terephthalate film (PMX727/36

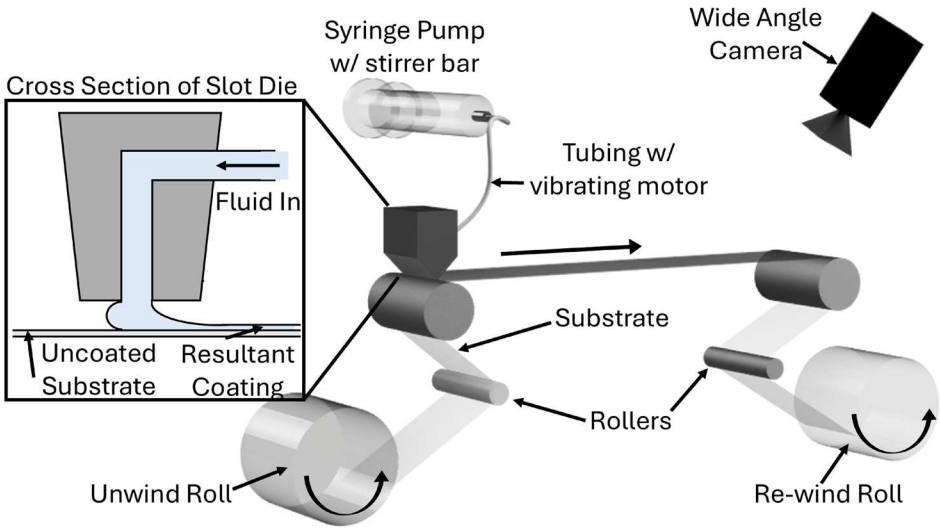


Fig. 7 Schematic of the roll-to-roll slot die coater. It is fitted with an inline wide angle camera, a magnetic stirrer bar in the syringe, with stirrer plate underneath, and a vibrating motor attached to the tubing connecting the syringe to the slot die. A cut through of the slot die is shown to aid visualisation of the internal fluid flow.

HiFi Films, United Kingdom) is unwound from a first roll, passed under a 10 mm wide stainless steel slot die (InfinityPV, Denmark), passed under an inline wide angle camera and then rewound onto a second roller. The substrate velocity, pump rate and coating gap were all computer controlled using custom made, LabView programs. A meniscus guide was used for all coatings.

Continuous stirring or agitation plays a critical role in maintaining a homogeneous suspension of colloidal particles, preventing sedimentation and aggregation that can otherwise prevent crystalline domains from forming. For example, Jenkins *et al.* vibrated tubing to prevent colloidal particle settling in the delivery tubing so the suspension reached the meniscus uniformly, which improved the coating uniformity of colloidal coating[42]. However, to date, continuous stirring or agitation has not been integrated with slot die coating processes for the fabrication of large-area monolayers of colloidal crystals.

We achieved the required agitation and stirring, using a vibrating motor (Seeed Studio, China) attached to the tubing between the slot die and syringe pump[42], using adhesive tape. A magnetic stirrer bar was also placed within the syringe, with an actuating magnetic stirrer plate (IKA, Germany) placed underneath.

A wide angle camera captured the appearance of the coating on the substrate with the optical setup shown in Supplementary Figs S1 and S2.

Scanning electron microscopy

Scanning electron microscopy images were obtained using an Inspect F (FEI, United States). Samples were cut out from the centre of the coated region, mounted onto stubs using carbon tape, gold coated and the corners of the substrate covered in silver paste to mitigate charge build up. SEM images of three 4 mm x 4 mm regions for each coating condition were used to assess uniformity and avoid sampling bias, and showed consistent colloidal packing behaviour. An accelerating voltage of 5 kV and a working distance of 10 mm was used for all images.

Voronoi plots and autocorrelation analysis

2D bond-orientational autocorrelation analysis was used to assess the quality of the manufactured colloidal crystal[43]. Scanning electron microscopy images capable of resolving individual colloidal xy positions were collected and underwent automatic particle detection. To enable this, the raw images were smoothed, had their contrast stretched and were then thresholded to isolate the particles. The image was then masked, keeping only the thresholded regions. The coordinates of the particle centres were then extracted. The centre-to-centre distances are

calculated and then the local orientational field of the hexatic order is also calculated. This local orientational field data is then plotted as a Voronoi plot[44].

Following the approaches of Lavergne *et al.*[45] and Ramananarivo *et al.*[43], the 2D bond-orientational autocorrelation function was calculated from the local bond-orientational order parameter $\psi_6(\vec{r}_j)$, which quantifies the local hexagonal ordering around each particle j. This parameter is defined as;

$$\psi_6(\vec{r}_j) = \frac{1}{N_j}\sum_{k=1}^{N_j} e^{i6\Delta\theta_{jk}}, \tag{1}$$

where $\Delta\theta_{jk}$ is the angle between the x-axis and the bond connecting the particle j to one of its N_j nearest neighbours k, determined using a Delaunay triangulation. The particles orientation in then given by;

$$\theta_6(\vec{r}_j) = \frac{1}{6}\arg\left(\psi_6(\vec{r}_j)\right), \tag{2}$$

and it varies from 0° to 60° due to the six-fold symmetry of the hexagonal lattice.

To quantify the decay of orientational order with distance, we computed the bond-orientational correlation function $\psi_6(\vec{r}_j)$. Prior to this calculation, the local order parameter $\psi_6(\vec{r}_i)$ was smoothed by averaging its value over the particles within the first two coordination shells surrounding each particle i. The resulting field, denoted $\psi_6(\vec{r}_i)$, was normalized to enhance the accuracy of short-range correlations. The spatial correlation function was then calculated as:

$$g_6(r) = \mathrm{Re}\left(\left\langle \hat{\psi}_6(\vec{r}+\vec{r}_0)\,\hat{\psi}_6^*(\vec{r}_0)\right\rangle\right), \tag{3}$$

where the term $\langle\cdot\rangle$ denotes the average over all the pairs of particles separated by a distance r. This function provides a measure of how the phase of the local bond-orientational order parameter is correlated across the sample. MATLAB 2026 was used to create the code for autocorrelation and image analysis, following the above approach. Voronoi plots were also made using MATLAB code.

Conclusions

This work demonstrates continuous roll-to-roll slot die coating as a method to manufacture large area colloidal crystal monolayers, which have significant potential to improve the performance of key advanced technologies including batteries and solar cells. Continuous slot die coating has well documented advantages as a manufacturing method, including predictable metering due to complete mass conservation, and overall demonstrated stability as a viable industrial process. As well as verifying the ability to produce high quality monolayers, our key finding is demonstrating roll-to-roll slot die coating's ability to change the areal coverage of colloids for a given formulation inline, by altering wet coating thickness by varying substrate speed relative to pump rate, to exert control over crystal packing. 2D bond-orientational autocorrelation order analysis was used to quantify the extent of long range order, and found to be well correlated with substrate velocity. This opens up the potential to use in-line metrology to determine order parameters and thereby enable self-optimising processes and sophisticated feedback and control loops, which may help to reach the exacting quality and crystallinity standards required for industrial manufacture. It is clear that there are many additional parameters that can influence colloid self-assembly during continuous slot-die coating, and the work here is presented as a first step towards a more comprehensive analysis. Within our study we have shown that while predictable and explainable colloid packing changes can be obtained and optimised within a certain parametric regime, the effect of increasing the magnitude of substrate velocity moved the system into a different response, with a change in packing type observed. In addition, our study is specific to one colloid size and type, and performed at a fixed temperature, conditions pragmatically optimised to encourage self-assembly. Significant work is required to generalise this approach to establish

a methodology capable of optimising colloidal self-assembly for different materials and sizes. However, the approach described here has significant potential to enable full Design of Experiments parametric investigations for a wider range of variables including size, polydispersity, composition and drying conditions, and consider the effect of altering the slot-die gap as well. Recently we have discussed how similar machine learning optimization, is a promising approach to speed up development of new materials and systems[41]. Future work to identify suitable proxy or direct metrics for order, including grazing incident small angle X-ray scattering may be insightful in this respect.

Although defects in the colloidal crystals were visible in some areas of samples, the use of less polydisperse colloids is expected to improve colloidal crystal quality. For example, in order to obtain the highest quality colloidal crystals, a polydispersity index of less than 2 % is required, significantly higher specification materials than reported here[46]. Additionally, combining slot die coating with techniques such as acoustic annealing may result in larger domain sizes[47].. Implementation of roll-to-roll slot die coating on commercial equipment with controlled environment and cleanliness is expected to produce further improvements in the material quality.

In summary it appears that roll-to-roll slot die coating is a viable method to continuously manufacture 2D colloidal crystals, and has the potential to be combined with optimisation and control approaches to increase the accessibility of these materials for future technological applications.

Supplementary Information The online version contains supplementary material available at https://doi.org/10.1038/s41598-026-71838-y.

Author contributions CP: Conceptualization, Methodology, Investigation, Writing - Original Draft and Visualization. AP Writing - Review & Editing. JH Writing - Review & Editing, Supervision, Funding acquisition. SE: Conceptualization, Writing - Review & Editing, Supervision, Funding acquisition.

Funding Electron microscopy was performed in the Sorby Centre for Electron Microscopy at the University of Sheffield. EPSRC grants EP/V051261/1 and EP/T004533/1.

Data availability Data is avaliablefrom corresponding author upon reasonable request.

Declarations

Competing interests The authors declare no competing interests.

Open Access This article is licensed under a Creative Commons Attribution 4.0 International License, which permits use, sharing, adaptation, distribution and reproduction in any medium or format, as long as you give appropriate credit to the original author(s) and the source, provide a link to the Creative Commons licence, and indicate if changes were made. The images or other third party material in this article are included in the article's Creative Commons licence, unless indicated otherwise in a credit line to the material. If material is not included in the article's Creative Commons licence and your intended use is not permitted by statutory regulation or exceeds the permitted use, you will need to obtain permission directly from the copyright holder. To view a copy of this licence, visit http://creativecommons.org/licenses/by/4.0/.

References

1. Xia, Y., Gates, B., Yin, Y. & Lu, Y. Monodispersed colloidal spheres: Old materials with new applications. *Adv. Mater.* **12**, 693–713. https://doi.org/10.1002/(SICI)1521-4095(200005)12:10%3C693::AID-ADMA693%3E3.0.CO;2-J (2000).
2. Astratov, V. N., Bogomolov, V. N., Kaplyanskii, A. A., Prokofiev, A. V. & Vlasov, A. A. Optical spectroscopy of opal matrices with cds embedded in its pores: Quantum confinement and photonic band gap effects. *Il Nuovo Cimento D* **17**, 1349–1354. https://doi.org/10.1007/BF02457208 (1995).
3. Vogel, N., Retsch, M., Fustin, C. A., del Campo, A. & Jonas U. Advances in colloidal assembly: The design of structure and hierarchy in two and three dimensions. *Chem. Rev.* **115**, 6265–6311. https://doi.org/10.1021/cr400081d (2015). **PMID: 26098223**.

4. Tran, V. T., Nguyen, H.-Q., Kim, Y.-M., Ok, G. & Lee, J. Photonic–plasmonic nanostructures for solar energy utilization and emerging biosensors. *Nanomaterials* **10**, 2248. https://doi.org/10.3390/nano10112248 (2020).
5. Armstrong, E. & O'Dwyer, C. Artificial opal photonic crystals and inverse opal structures – fundamentals and applications from optics to energy storage. *J. Mater. Chem. C* **3**, 6109–6143. https://doi.org/10.1039/C5TC01083G (2015).
6. Mihi, A., López-Alcaraz, F. J. & Míguez, H. Full spectrum enhancement of the light harvesting efficiency of dye sensitized solar cells by including colloidal photonic crystal multilayers. *Appl. Phys. Lett.* **88**, 193110. https://doi.org/10.1063/1.2200746 (2006).
7. Bhardwaj, R., Fang, X., Somasundaran, P. & Attinger, D. Self-assembly of colloidal particles from evaporating droplets: Role of dlvo interactions and proposition of a phase diagram. *Langmuir* **26**, 7833–7842. https://doi.org/10.1021/la904727 (2010). **PMID: 20337481**.
8. Pusey, P. N. et al. Hard spheres: crystallization and glass formation. *Philos. Trans. R. Soc. A: Math. Phys. Eng. Sci.* **367**, 4993–5011. https://doi.org/10.1098/rsta.2009.0181 (2009).
9. Liu, L., Karuturi, S. K., Su, L. T. & Tok, A. I. Y. Tio2 inverse-opal electrode fabricated by atomic layer deposition for dye-sensitized solar cell applications. *Energy Environ. Sci.* **4**, 209–215. https://doi.org/10.1039/C0EE00086H (2011).
10. Liu, Z. et al. Three-dimensional ordered porous electrode materials for electrochemical energy storage. *NPG Asia Materials* **11**, 12. https://doi.org/10.1038/s41427-019-0112-3 (2019).
11. Zheng, G. et al. Interconnected hollow carbon nanospheres for stable lithium metal anodes. *Nat. Nanotechnol.* **9**, 618–623. https://doi.org/10.1038/nnano.2014.152 (2014).
12. Cai, Z. et al. From colloidal particles to photonic crystals: advances in self-assembly and their emerging applications. *Chem. Soc. Rev.* **50**, 5898–5951. https://doi.org/10.1039/D0CS00706D (2021).
13. Wan, Y. & Qian, W. From self-assembly of colloidal crystals toward ordered porous layer interferometry. *Biosensors* **13** (730), 13. https://doi.org/10.3390/bios13070730 (2023). **Published 2023 Jul 13**.
14. Ye, X. et al. Monolayer colloidal crystals by modified air-water interface self-assembly approach. *Nanomaterials* **7**, 291. https://doi.org/10.3390/nano7100291 (2017).
15. Toolan, D. T. W., Fujii, S., Ebbens, S. J., Nakamura, Y. & Howse, J. R. On the mechanisms of colloidal self-assembly during spin-coating. *Soft Matter* **10**, 8804–8812. https://doi.org/10.1039/C4SM01711K (2014).
16. Qdemat, A. et al. Self assembled monolayer of silica nanoparticles with improved order by drop casting. *RSC Adv.* **10**, 18339–18347. https://doi.org/10.1039/d0ra00936a (2020).
17. Kohoutek, T., Parchine, M., Bardosova, M., Fudouzi, H. & Pemble, M. Large-area flexible colloidal photonic crystal film stickers for light trapping applications. *Opt. Mater. Express* **8**, 960–967. https://doi.org/10.1364/OME.8.000960 (2018).
18. Parchine, M., McGrath, J., Bardosova, M. & Pemble, M. E. Large area 2d and 3d colloidal photonic crystals fabricated by a roll-to-roll langmuir-blodgett method. *Langmuir* **32**, 5862–5869. https://doi.org/10.1021/acs.langmuir.6b01242 (2016). **Epub 2016 Jun 1**.
19. Bardosova, M., Pemble, M. E., Povey, I. M. & Tredgold, R. H. The Langmuir-Blodgett approach to making colloidal photonic crystals from silica spheres. *Adv. Mater.* **22**, 3104–3124. https://doi.org/10.1002/adma.200903708 (2010).
20. Niederberger, M. Multiscale nanoparticle assembly: From particulate precise manufacturing to colloidal processing. *Adv. Funct. Mater.* **27**, 1703647. https://doi.org/10.1002/adfm.201703647 (2017).
21. Cagnani, G. R. et al. Large-area flexible 2d-colloidal crystals produced directly using roll-to-roll processing. *Colloids Surf. A: Physicochem. Eng. Asp.* **588**, 124389. https://doi.org/10.1016/j.colsurfa.2019.124389 (2020).
22. Yang, H. & Jiang, P. Large-scale colloidal self-assembly by doctor blade coating. *Langmuir* **26**, 13173–13182. https://doi.org/10.1021/la101721v (2010). **PMID: 20695556**.
23. Rengarajan, R., Mittleman, D., Rich, C. & Colvin, V. Effect of disorder on the optical properties of colloidal crystals. *Phys. Rev. E* **71**, 016615. https://doi.org/10.1103/PhysRevE.71.016615 (2005).
24. Liu, T., Young, C. M., Moore, T. C., Glotzer, S. C. & Solomon, M. J. Defect structures in colloidal crystals and their effect on grating diffraction structural color. *ACS Appl. Mater. Interfaces*. **17**, 8171–8182. https://doi.org/10.1021/acsami.4c18558 (2025). **PMID: 39841887**.
25. Reck, F. E. & Browning, C. W. Coating apparatus and method. https://patents.google.com/patent/US2710275A (1955). US Patent 2,710,275. Assigned to Eastman Kodak Co. Filed Nov 27, 1951; issued Jul 5, 1955.
26. Tanwar, J., Vinjamur, M. & Scriven, L. E. Design principles of integrated vacuum slot arrangement. *AIChE J.* **53**, 572–578. https://doi.org/10.1002/aic.11112 (2007).
27. Ding, X., Liu, J. & Harris, T. A. L. A review of the operating limits in slot die coating processes. *AIChE J.* **62**, 2508–2524. https://doi.org/10.1002/aic.15268 (2016).
28. Lee, S. & Nam, J. Analysis of slot coating flow under tilted die. *AIChE J.* **61**, 1745–1758. https://doi.org/10.1002/aic.14752 (2015).
29. Romero, O. & Carvalho, M. Response of slot coating flows to periodic disturbances. *Chem. Eng. Sci.* **63**, 2161–2173. https://doi.org/10.1016/j.ces.2008.01.012 (2008).
30. Pusey, P. Liquids, freezing and glass transition. *Les Houches Session* **51**(1989), 765–942 (1991).
31. Royall, C. P., Leunissen, M. E., Hynninen, A.-P., Dijkstra, M. & van Blaaderen, A. Re-entrant melting and freezing in a model system of charged colloids. *J. Chem. Phys.* **124**, 244706. https://doi.org/10.1063/1.2189850 (2006).

32. Cates, M. E., Wittmer, J. P., Bouchaud, J.-P. & Claudin, P. Jamming, force chains, and fragile matter. *Phys. Rev. Lett.* **81**, 1841–1844. https://doi.org/10.1103/PhysRevLett.81.1841 (1998).
33. Lotito, V. & Zambelli, T. Approaches to self-assembly of colloidal monolayers: A guide for nanotechnologists. *Adv. Colloid Interface Sci.* **246**, 217–274. https://doi.org/10.1016/j.cis.2017.04.003 (2017).
34. Pan, S. et al. Simulation analysis of the influence of operating parameters on the pressure profile in the coating bead. *Coatings* **14**, 1413. https://doi.org/10.3390/coatings14111413 (2024).
35. Deegan, R. D. et al. Capillary flow as the cause of ring stains from dried liquid drops. *Nature* **389**, 827–829. https://doi.org/10.1038/39827 (1997).
36. Monovoukas, Y. & Gast, A. P. The experimental phase diagram of charged colloidal suspensions. *J. Colloid Interface Sci.* **128**, 533–548. https://doi.org/10.1016/0021-9797(89)90368-8 (1989).
37. Roach, L. et al. Controlling disorder in self-assembled colloidal monolayers via evaporative processes. *Nanoscale* **14**, 3324–3345. https://doi.org/10.1039/d1nr07814c (2022).
38. Arif, M., Schofield, A. B., Laidlaw, F. H. J., Poon, W. C. K. & Thijssen, J. H. J. Impact of particle-size polydispersity on the quality of thin-film colloidal crystals. *Soft Matter* https://doi.org/10.1039/D5SM00754B (2025).
39. Auer, S. & Frenkel, D. Suppression of crystal nucleation in polydisperse colloids due to increase of the surface free energy. *Nature* **413**, 711–713. https://doi.org/10.1038/35099513 (2001).
40. Tang, Z., Rossiter, J. & Panoutsos, G. Disturbance observer-based optimal tracking control for slot coating process with mismatched input disturbances (2024). 2024 The Author(s).
41. Passmore, C., Wu, K., Howse, J., Panoutsos, G. & Ebbens, S. Surrogate-assisted optimization of roll-to-roll slot die coating. *Sci. Rep.* **15**, 29185. https://doi.org/10.1038/s41598-025-11279-1 (2025). **Published online 9 August (2025)**.
42. Jenkins, J. S., Flickinger, M. C. & Velev, O. D. Continuous convective-sedimentation assembly of colloidal microsphere coatings for biotechnology applications. *Coatings* **3**, 26–48. https://doi.org/10.3390/coatings3010026 (2013).
43. Ramananarivo, S., Ducrot, E. & Palacci, J. Activity-controlled annealing of colloidal monolayers. *Nat. Commun.* **10**, 3380. https://doi.org/10.1038/s41467-019-11362-y (2019).
44. Lotito, V. & Zambelli, T. Pattern detection in colloidal assembly: A mosaic of analysis techniques. *Adv. Colloid Interface Sci.* **284**, 102252. https://doi.org/10.1016/j.cis.2020.102252 (2020).
45. Lavergne, F. A., Aarts, D. G. A. L. & Dullens, R. P. A. Anomalous grain growth in a polycrystalline monolayer of colloidal hard spheres. *Phys. Rev. X.* **7**, 041064. https://doi.org/10.1103/PhysRevX.7.041064 (2017).
46. Wong, S., Kitaev, V. & Ozin, G. A. Colloidal crystal films: Advances in universality and perfection. *J. Am. Chem. Soc.* **125**, 15589–15598. https://doi.org/10.1021/ja0379969 (2003).
47. He, G. et al. Regulating two-dimensional colloidal crystal assembly through contactless acoustic annealing. *J. Appl. Phys.* **135**, 145304. https://doi.org/10.1063/5.0185692 (2024). https://pubs.aip.org/aip/jap/article-pdf/doi/10.1063/5.0185692/19877219/145304_1_5.0185692.pdf.

Publisher's note Springer Nature remains neutral with regard to jurisdictional claims in published maps and institutional affiliations.

Authors and Affiliations

Christopher Passmore[1] · Andrew J. Parnell[2] · Jonathan R. Howse[1] · Stephen J. Ebbens[1]

✉ Stephen J. Ebbens
s.ebbens@sheffield.ac.uk

[1] School of Chemical, Materials and Biological Engineering, The University of Sheffield, Mappin St, Sheffield, United Kingdom

[2] School of Mathematical and Physical Sciences, The University of Sheffield, Hounsfield Road, Sheffield, United Kingdom